Available online at www.sciencedirect.com
ScienceDirect
Journal of Power Sources 170 (2007) 111–121
JOURNAL OF POWER SOURCES
www.elsevier.com/locate/jpowsour

Experimental investigation of the role of a microporous layer on the water transport and performance of a PEM fuel cell

Hasan K. Atiyeh [1], Kunal Karan *, Brant Peppley, Aaron Phoenix [2], Ela Halliop, Jon Pharoah

Queen's-RMC Fuel Cell Research Centre, Kingston, Ont., Canada K7L 5L9

Received 20 February 2007; received in revised form 29 March 2007; accepted 3 April 2007
Available online 13 April 2007

Abstract

A highly reliable experimental system that consistently closed the overall water balance to within 5% was developed to study the role of a microporous layer (MPL), attached to carbon paper porous transport layer (PTL), on the water transport and performance of a standard 100 cm^2 active area PEM fuel cell. Various combinations of cells were built and tested with PTLs at the electrodes using either carbon fibre paper with a MPL (SGL 10BB) or carbon fibre paper without a MPL (SGL 10BA). The net water drag coefficient at three current densities (0.3, 0.5 and 0.7 A cm^{-2}) for two combinations of anode/cathode relative humidity (60/100% and 100/60%) and stoichiometric ratios of H_2/air (1.4/3 and 1.4/2) was determined from water balance measurements. The addition of a MPL to the carbon fibre paper PTL at the cathode did not cause a statistically significant change to the overall drag coefficient although there was a significant improvement to the fuel cell performance and durability when a MPL was used at the cathode. The presence of a MPL on either electrode or on both electrodes also exhibited similar performance compared to when the MPL was placed at the cathode. These results indicate that the presence of MPL indeed improves the cell performance although it does not affect the net water drag coefficient. The correlation between cell performance and global water transport cannot be ascertained and warrants further experimental investigation.

Keywords: PEM fuel cell; Water transport; Microporous layer; Net water drag; Ionomeric membrane

1. Introduction

Water management in a polymer electrolyte membrane fuel cell (PEMFC) is key in achieving high performance and efficient operation of the fuel cell [1–3]. Whereas the PEM needs to be fully hydrated to ensure high proton conductivity, it is crucial to remove excess liquid water generated at the cathode to avoid flooding of the catalyst layer and porous transport layer (PTL) [4], which is often referred to as the gas diffusion layer (GDL). The PTL bridges the catalyst layer and the flow-field plates (FFP) in the PEMFC. Excessive flooding of the cathode catalyst layer impedes oxygen transport to the active sites resulting in an increased mass transport limitation, which is manifested via lowering of the limiting current densities. Further, depending on the humidification level of the reactant feed streams, localized drying of the membrane can occur leading to excessive ohmic heating and, ultimately, to pinhole formation in the membrane. Therefore, improper water management may not only compromise fuel cell performance but also contribute to a rapid degradation of the membrane electrode assembly (MEA) of a PEMFC.

There is no universally applicable strategy for water management in PEMFCs because water transport in various components of a PEMFC is affected by the operating conditions such as feed stream humidification level, operating temperature, and reactant stoichiometric ratio as well as by the physical characteristics of the fuel cell components, especially that of the PTL [5]. To improve water transport, the PTL is treated with a hydrophobic material such as Teflon to change its wetting characteristics. Such a treatment leads to pockets of hydrophilic and hydrophobic pores in the PTL [6,7]. It is thought that

* Corresponding author. Tel.: +1 613 533 3095; fax: +1 613 533 6637.
E-mail address: karan@chee.queensu.ca (K. Karan).
[1] Current address: Department of Chemical Engineering, King Saud University, P.O. Box 800, Riyadh 11421, Saudi Arabia.
[2] Permanent address: Department of Chemical Engineering, University of Saskatchewan, Saskatoon, Sask., Canada S7N 5A9.

0378-7753/$ – see front matter © 2007 Elsevier B.V. All rights reserved.
doi:10.1016/j.jpowsour.2007.04.016

hydrophobic regions allow a pathway for gas transport whereas the hydrophilic regions facilitate liquid transport. In addition to the hydrophobic treatment of the PTL, the use of a surface layer or microporous layer (MPL) has become a common practice [6]. The MPL is usually made of a mixture of carbon particles and a hydrophobic agent coated on one side of the conventional PTL. The MPL pore size range is 0.1–0.5 μm compared to that of the PTL whose range is 10–30 μm. It is thought that the MPL provides effective wicking of liquid water from the catalyst layer into the diffusion media [6].

It is clear that water transport and management in PEMFCs depends on several variables of which the reactant stream humidification, the structural characteristics of PTL, and, if present, the MPL and its structural characteristics are important. Previous studies have investigated different aspects of the water transport in PEMFCs to varying extent. Early modeling studies were concerned with the influence of reactant stream humidification on water flooding [8–11]. These models were pseudo-single phase and did not have separate equations to describe liquid-phase transport. Later, two-phase models accounted for this effect which allowed for a more realistic representation of liquid water transport [12–14].

A further improvement was implemented by Nam and Kaviany [15], who accounted for the presence of hydrophobic regions in the PTL unlike earlier models that assumed the PTL to be composed of hydrophilic material only. They presented computational results for a system in which a MPL was placed between the cathode catalyst layer and the PTL. The MPL considered in their model was fibrous in nature. The placement of the MPL helped in reducing water saturation in the adjacent catalyst layer. Passaogullari and Wang [16] reported similar findings. However, both studies [15,16] were based on half-cell models and considered water transport in the PTL/MPL only but did not include the membrane in the model. As such, the role of the MPL on the overall water transport and its effect on the net water drag coefficient was not investigated. Weber and Newman [17] employed a two-phase, 2D, fuel cell model to study the influence of the MPL on water transport. They fitted key model parameters to the experimental data of Qi and Kaufman [18], who had reported PEMFC performance for single-cells with and without a MPL. The structural parameters of the PTL and MPL (PTL porosity, MPL porosity and MPL fraction of hydrophobic pores) were used as adjustable parameters to fit their 2D model to the single-cell polarization curves reported by Qi and Kaufman [18]. Based on the predictions from the tuned model, they claimed that the MPL acts as a valve that pushes water away from the cathode PTL through the membrane to the anode.

Lin and Nguyen [19] have recently investigated the effect of MPLs on PEMFC performance for several PTLs. They observed that PEMFCs with a MPL exhibited better performance than the fuel cells without a MPL. They hypothesized that the MPL helps keep liquid water in the cathode catalyst layer and minimizes liquid water transport to the cathode PTL. That is, the MPL increases the back-diffusion rate of water from the cathode through the membrane to the anode. Interestingly, this hypothesis, although in agreement with Weber and Newman's modeling result is in contrast to the simulation results of Nam and Kaviany [15] and Pasaogullari and Wang [16], both of whom showed that the MPL enhances water removal rate from the catalyst layer to the cathode PTL. In a later work, Pasaogullari et al. [20] developed a 1D, two-phase unit cell model to study the effects of MPL and its properties on water transport considering both anode and cathode as well as the membrane. It was shown that hydraulic pressure build up due to strong capillary pressure in the MPL results in a higher pressure differential across the membrane which enhances the water transport from the cathode to the anode. The back-flow of water was found to be a function of several MPL parameters—hydrophobicity, thickness, pore size and porosity. These studies [15–20] clearly present contrasting explanation on the role of MPL on the water transport and neither one has reported nor used experimental data from water balances to support their hypothesis.

The published work on MPLs is mostly focused on the effect of composition and preparation methods on PEMFCs performance [18,21–26]. Fewer studies were reported on experimental data of water transport in an operating PEMFC using a water balance [27–31]. Experimental data on water transport are usually discussed in terms of net water drag coefficient, i.e. the moles of water dragged from anode through the membrane to the cathode per mole of proton transported. The effect of humidification level of reactants and current density [27–31], membrane thickness [28,30], pressure [28,29], cell temperature and stoichiometric ratio of H_2/air [28,29] on the net water drag have been studied. All studies showed that the net water drag can be affected by the operating conditions. A lower net water drag coefficient was observed when the cathode was at a higher humidification level than the anode [27–31]. A lower drag coefficient was obtained when a thinner membrane was used compared to a thicker member [28,30]. Among the previous studies, Janssen and Overvelde [28] presented net drag coefficients for a wide range of operating conditions such as current density, temperature, pressure, stoichiometry and humidity of the inlet gases, which were either fully saturated or dry. They also reported data for different types of MEAs, though none using catalyst coated membranes (CCM). Neither of the other two reports on water transport determination by water balance experiments for PEMFCs with a MPL used CCMs [30,31]. This is significant since one of the early hypotheses for the performance improvements due to presence of a MPL was that it kept the catalyst layer from penetrating the PTL substrate. Janssen and Overvelde [28] found that the humidity and the stoichiometry of the inlet gases had a much larger effect on the drag than did the different fuel cell components. They also examined the effect of the MPL on PEMFC performance and water transport to a varying extent. However, the PTL type and/or the catalyst loading for any two sets of their experiments were different. Unfortunately, not a single set of data was reported that would allow a direct investigation of the effects of MPL solely on water drag coefficient.

In summary, the role of a MPL on water transport in PEMFCs remains unresolved. An absence of experimental data in open literature on the water balance across the PEMFC has perpetuated the confusion on whether the role of a MPL is to enhance back-diffusion of water from the cathode through the membrane to the anode or to improve water removal from the cathode catalyst

layer through the MPL to the PTL. Thus, the primary objective of this study was to obtain reliable experimental data that can help resolve the question: whether, how and to what extent does the MPL on either electrode or on both electrodes affect water transport in PEMFCs? A secondary but essential objective was to develop an experimental system and protocol such that reliable water balance data could be generated.

Recently, we reported the first set of experimental results on the effect of MPL on the net drag coefficient of water from the anode through the membrane to the cathode and on fuel cell performance when the MPL was only present at the cathode side [32]. The net drag coefficient was determined from water balance measurements. In this study, we report results on the influence of a MPL, when it is used at either electrode or at both electrodes, on the net drag coefficient at various operating conditions. The effect of humidification level of reactants, current density and stoichiometric ratio of H_2/air were investigated.

2. Experimental

2.1. Fuel cell components

The flow field plate (FFP) used for the anode and cathode sides of the fuel cell were similar, each having seven serpentine parallel channels. Catalyst coated membranes (CCMs) with Nafion 112 and 0.3 mg cm^{-2} platinum catalyst loading on each electrode (Ion Power, USA) were used. All experiments were conducted in a single cell with a total active area of 100 cm^2. Two types of porous transport layer (PTL), SGL 10BA and SGL 10BB carbon papers (SGL Carbon Group, USA), were investigated. The typical properties of the SGL carbon papers used in the present study can be found on the supplier website [33]. The SGL10 BA carbon paper was treated with 5 wt% PTFE. The SGL 10BB carbon paper has a microporous layer (MPL) on one face. The PTFE content of the MPL was 23%. The thicknesses of the 10BA and 10BB carbon papers were 0.37 and 0.41 mm, respectively. The PTLs and the MEAs from the same batch were used in the tests to minimize variability in physical and chemical characteristics of fuel cell components. Two types of sealing gaskets, silicone coated fabric (0.26 mm thick) and Teflon coated glass fabric (0.07 mm thick) (Green Belting Industries, Canada), were used. The silicone coated fabric gasket was used to seal the fuel cell when SGL 10BA carbon paper was used. However, both gaskets were employed with the SGL 10BB carbon paper because of the increased thickness of the PTL with a MPL.

2.2. Fuel cell assembly

A very rigorous procedure for fuel cell assembly was developed and implemented to ensure reproducibility. The sealing gaskets and PTLs were cut using a die cutter. The sealing gaskets and FFPs were then first cleaned with methanol and then with DI water. They were then dried with dry-filtered and oil-free compressed air. The PTLs and CCMs were visually inspected to ensure absence of cracks or holes before use.

The fuel cell components were assembled as follows: (1) the cathode FFP was aligned and placed onto the cathode bus bar attached to the endplate, (2) the sealing gasket was centered on the FFP, (3) the PTL was positioned within the sealing gasket's center opening such that the MPL, when used, will be facing the CCM, (4) the CCM was centered on the assembly, (5) another sealing gasket was centered on the assembly, (6) another PTL was positioned within the sealing gasket's center opening such that the MPL, when used, will face the anode side of the CCM, (7) the anode FFP was placed on top of the assembly, (8) the other endplate with the anode bus bar was aligned and placed on the assembly and (9) the fuel cell was clamped with eight bolts while a hydraulic press (Enerpac RC1010, USA) was used to provide a uniform compression on the cell. The average compression in the cell was about 960 kPa.

The assembled fuel cell was pressurized with air at 51 kPa and leak tested. The cell was considered acceptable for testing if three main criteria were met: no crossover leaks, anode and/or cathode leaks of less than 1.0 ml min^{-1} and an internal resistance lower than 20 mΩ. A Gilmont Flow meter F-4001 (Gilmont Instruments, USA) was used to measure the gas leak rate. The internal cell resistance was measured by Hioki 3560 HiTester (Hioki Co., Japan) at a frequency of 1 kHz. The fuel cell was operated in counter flow configuration. The inlet and outlet streams from the fuel cell as well as the locations of the cartridge heaters and thermocouple used for feedback control of the cartridge heaters are shown in Fig. 1.

2.3. Fuel cell test system

Tests were conducted on an automated fuel cell test station (Hydrogenics FCATS-S800). This test station is equipped with temperature controllers for the fuel cell, humidifiers and gas lines. It is also equipped with a primary water collection system for both anode and cathode effluent streams. Each primary water collection system consists of a knockout drum and a collection vessel connected to a differential pressure transducer (DPT) and solenoid valve (SV) as shown for the cathode effluent in Fig. 2. The DPT activates the SV to open when the condensed water level in the collection vessel reaches a preset height allowing water to flow out into a collection flask. The time to fill the

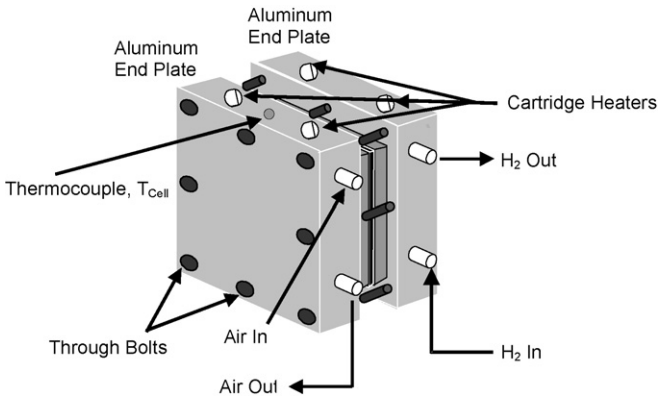

Fig. 1. Schematic diagram of the fuel cell used.

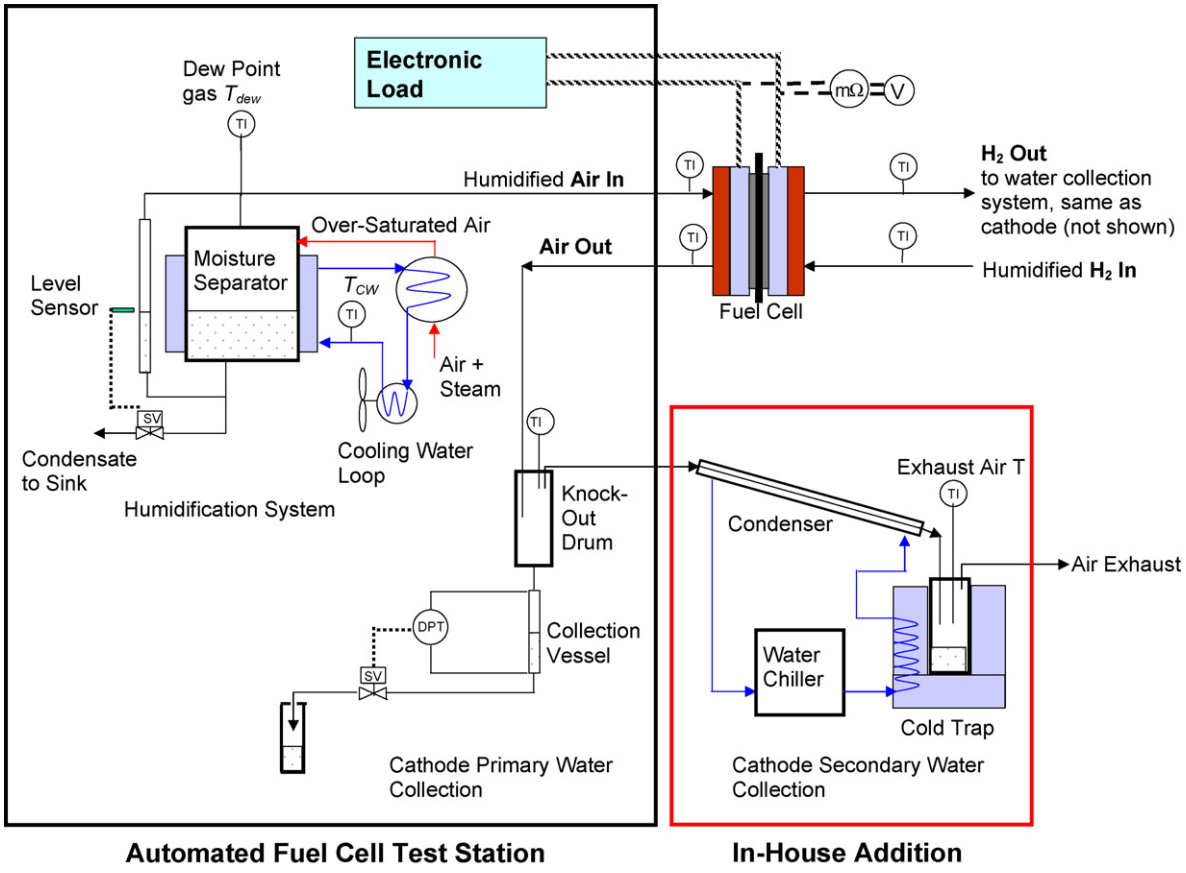

Fig. 2. Schematic diagram of experimental setup used.

collection vessel to the level needed to actuate the SV to open varies based on the operating conditions.

Preliminary water balance measurements showed that the standard humidification configuration and primary water collection systems did not provide sufficiently accurate results for a meaningful calculation of the net water drag coefficient. This was mainly due to the way the gas dew point temperature was set and controlled on the automated test system as well as due to the variations in the temperature around the air-cooled knockout drum located inside the test station cabinet. As delivered, the automated test station used the circulating water temperature (T_{CW} in Fig. 2) in the moisture separator as an estimate of the gas dew point temperature for controlling the gas stream relative humidity (RH). However, it was found that T_{CW} was 3–8 °C higher than the gas temperature leaving the moisture separator to the fuel cell. Consequently, the system was modified to use temperature of the gas leaving the moisture separator (T_{dew} in Fig. 2) to better control the RH of the gas streams entering the fuel cell.

In order to obtain reliable measurements, a secondary water collection system was built in-house. The secondary water collection systems condensed the water from the gases leaving the knockout drums using a condenser and a cold trap. This resulted in a more accurate water balance that was verified experimentally. Following these modifications, the overall water balance consistently closed to within 5%. The absolute average relative error in the water balance was 1.5% for all tests performed. The primary and secondary collection systems for the anode effluent stream are similar to the cathode side but are not shown in Fig. 2.

2.4. Water balance experimental conditions

The net drag coefficient was determined from water balance measurements for each fuel cell build (Table 1) at three current densities (0.3, 0.5 and 0.7 A cm^{-2}) and under two different anode/cathode (A/C) RH (60/100% and 100/60%) and two combinations of stoichiometric ratios of H_2/air (1.4/3 and 1.4/2). The test runs at a stoichiometric ratio of H_2/air of 1.4/2 were conducted on the same cell builds after completion of experiments at a stoichiometric ratio of H_2/air of 1.4/3 and confirming that the fuel cell performance remained similar to the performance

Table 1
Experimental fuel cell builds

Cell builds	Cell builds rejected[a]	Anode PTL[b]	Cathode PTL[b]
A1[c]–A3	–	SGL 10BA	SGL 10BB
B1[c]–B8	B3, B5, B7, B8	SGL 10BA	SGL 10BA
C1 and C2	C1	SGL 10BB	SGL 10BA
D1 and D2	–	SGL 10BB	SGL 10BB

[a] Runs discarded because beginning of life cell voltage was less than 0.4 V at 0.7 A cm^{-2}.
[b] 10BA without a MPL; 10BB with a MPL.
[c] Cell builds A1 and B1 were used for commissioning of the water balance system.

just after initial conditioning. This was verified using standard polarization measurements that will be discussed in the next section. Pure H_2 and air were supplied to the anode and cathode, respectively, in a current based flow control mode. The supply pressures to the anode and cathode were maintained at 35 kPa.

The inlet gas temperatures and cell temperature were controlled at a nominal value of 60 °C. Lines between humidifiers and the fuel cell were heated to avoid condensation. The cell voltage, current, H_2 and air flow rates, inlet dew point gas temperatures, inlet and outlet gas temperatures and pressures of the anode and cathode streams along with the exhaust gas temperatures from the primary and secondary water collection systems were recorded using the data acquisition software supplied with the fuel cell test station. The internal cell resistance was also recorded with the software supplied with the Hioki HiTester. At the end of each run, the water collected from the primary and secondary collection systems of the anode and cathode was weighed and recorded.

2.5. Fuel cell performance monitoring

The fuel cell performance was monitored using standard polarization measurements at a nominal operating temperature of 60 °C, inlet pressure of 35 kPa, and at 100% RH for both inlet gases. The stoichiometric ratios of H_2 and air were 1.4 and 3, respectively. It should be noted that these standard polarization measurements were made at different conditions than those used to investigate the role of the MPL on water transport in that the RH of A/C feed streams was 100%. Polarization curves were generated for each cell built after initial conditioning and at the end of the water transport experiments. Several fuel cell builds without a MPL and only one build with a MPL at the anode were discarded because they did not meet the beginning of life critical performance, a cell voltage greater than 0.4 V at 0.7 A cm^{-2} (Table 1).

3. Calculation and error analysis

An overall water balance was performed around the fuel cell, accounting for the water generated from the overall H_2–O_2 reaction, to assess the reliability of the experimental results. An overall water balance was considered "closed" when the difference between the "water in + generation" and the "water out" was less than the 95% confidence limits of the calculation. In the calculations, the RH of a stream was determined from the ratio of the saturation pressure at the dew point temperature (T_{dew}) and the saturation pressure at the nominal cell temperature (T_{cell}):

$$\mathrm{RH} = \frac{P_{sat}(T_{dew})}{P_{sat}(T_{cell})} \quad (1)$$

where the dew point temperatures correspond to the measured temperature of the gas stream leaving the moisture separator (see Fig. 2) and the saturation pressure was determined from standard thermodynamic correlations.

The net water drag coefficient, α (mol H_2O (mol H^+)$^{-1}$), was calculated solely from a water balance performed on the cathode side of the fuel cell:

$$\alpha = \frac{F(W_{out} - W_{in}) - iA/2}{iA} \quad (2)$$

where F is the Faraday constant (96,487 C mol^{-1}), W_{in} the cathode-side inlet water flow rate (mol s^{-1}), W_{out} the cathode-side outlet water flow rate (mol s^{-1}), i the current density (A cm^{-2}), and A is the total active electrode area (cm^2). The cathode-side inlet water flow rate, W_{in} (mol s^{-1}), is calculated from the known dry air flow rate and RH while the cathode-side outlet water flow rate, W_{out} (mol s^{-1}), is determined from liquid water collected at the cathode primary collector and cold trap, and the water vapor passing through the cold trap:

$$W_{out} = W_{liq,coll} + W_{liq,trap} + W_{vap,\,trap} \quad (3)$$

where $W_{liq,coll}$ is the liquid water collected in the primary water collection system divided by the cumulative run time (mol s^{-1}), $W_{liq,trap}$ is the liquid water collected in the cold trap divided by the cumulative run time (mol s^{-1}), and $W_{vap,trap}$ is the water vapor vented from the cold trap (mol s^{-1}). $W_{vap,trap}$ was calculated on the assumption that the vapor leaving the cold trap was at its dew point temperature. The assumption that the exhaust gas stream leaving the cold trap was saturated with water vapor at the measured cold trap temperature was verified in separate experiments.

The 95% confidence limits in the data and calculated results are based only on the uncertainty associated with the standard deviations of the measured variables and conservative estimates of the uncertainty in the mass of liquid water collected. Temperature fluctuations were the main contributors in the reported experimental uncertainty due to their effect on the vapor pressure of water. Where multiple runs of the same build were performed, the results were averaged and the appropriate decreased uncertainty was reported. Experimental variations associated with the CCM, the PTL, the MPL and the build process can be seen directly from the experimental results.

4. Results and discussion

4.1. Fuel cell performance at standard conditions

Standard polarization curves for all configurations tested (Table 1) are shown in Fig. 3(a) and (b). Individual plots correspond to the polarization curves for each build after initial conditioning and at the end of the water transport experiments. It can be readily seen that the polarization curves for the cells with a MPL on either electrode (builds A2, A3 and C2) or on both electrodes (builds D1 and D2) in Fig. 3a show a more consistent and in general better performance than those without a MPL (builds B2, B4 and B6) in Fig. 3b. Furthermore, cells with a MPL showed very little deterioration in performance between the initial and final polarization curves (an average of 570 h of operation). Cells without a MPL (Fig. 3b) exhibited more variability in post conditioning performance and a clear degradation between the post conditioning and final polarization curves (an average of 250 h of operation). All of the cell builds with a MPL present at the cathode by itself or in combination with a MPL

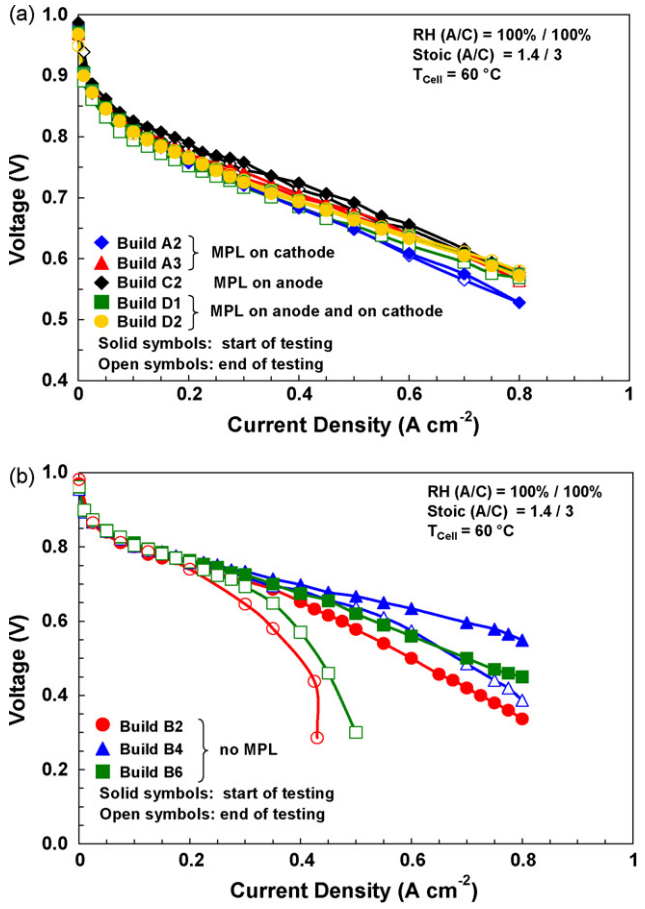

Fig. 3. Standard polarization curves for (a) builds with a MPL and (b) builds without a MPL. Solid symbols start of testing; open symbols at end of testing.

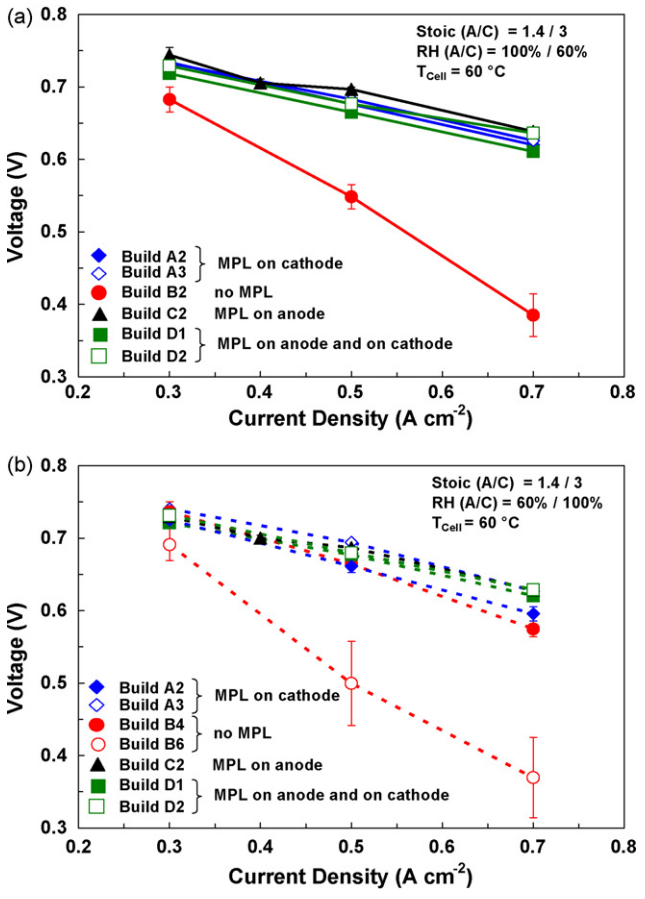

Fig. 4. Cell performance curves for builds with various combinations of porous transport layers at stoichiometric ratio of H_2/air of 1.4/3 for (a) anode/cathode relative humidity of 100/60% and (b) anode/cathode relative humidity of 60/100%. Error bars not visible are smaller than the symbols.

at the anode met the beginning of life critical performance of a cell voltage higher than 0.4 V at 0.7 A cm^{-2} (Table 1). However, several builds without a MPL and only one cell build with a MPL on the anode were discarded because they did not meet the beginning-of-life critical performance.

4.2. Fuel cell performance at water balance conditions

Figs. 4 and 5 show the cell voltage measured at various current densities and under two different anode/cathode relative humidities (A/C RH) (60/100% and 100/60%) and a stoichiometric ratios of H_2/air of 1.4/3 and 1.4/2. Cell builds without a MPL (builds B, Table 1) were unstable to operate at the lower stoichiometric ratio. Most of the data in Figs. 4 and 5 include at least one repeat experiment with the same cell build, which are averaged. It is clear that, with one exception, the data groups according to the presence of a MPL resulting in significantly enhanced performance, especially at higher current densities (Fig. 4a and b). It is not clear why one cell build without a MPL (build B4) exhibited performance similar to those cells with a MPL under water balance conditions (Fig. 4b) and also the lowest rate of performance deterioration (Fig. 3b). This may suggest that the MPL facilitates the assembly of the fuel cell even though considerable care was taken in the assembly of all cells. The fuel cell performance was in general slightly lower when the stoichiometric ratio of H_2/air was 1.4/2 (Fig. 5) compared to 1.4/3 (Fig. 4). A similar performance was obtained whether the MPL was used on either the anode or cathode or on both electrodes. In addition, the cell voltage was not affected by the inlet humidification conditions

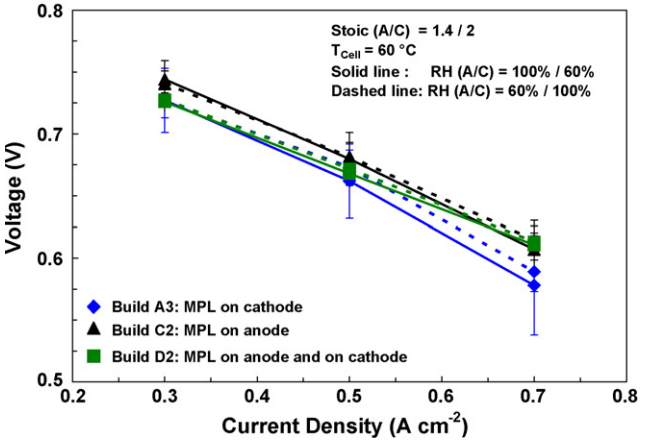

Fig. 5. Cell performance curves for builds with various combinations of porous transport layers at stoichiometric ratio of H_2/air of 1.4/2.

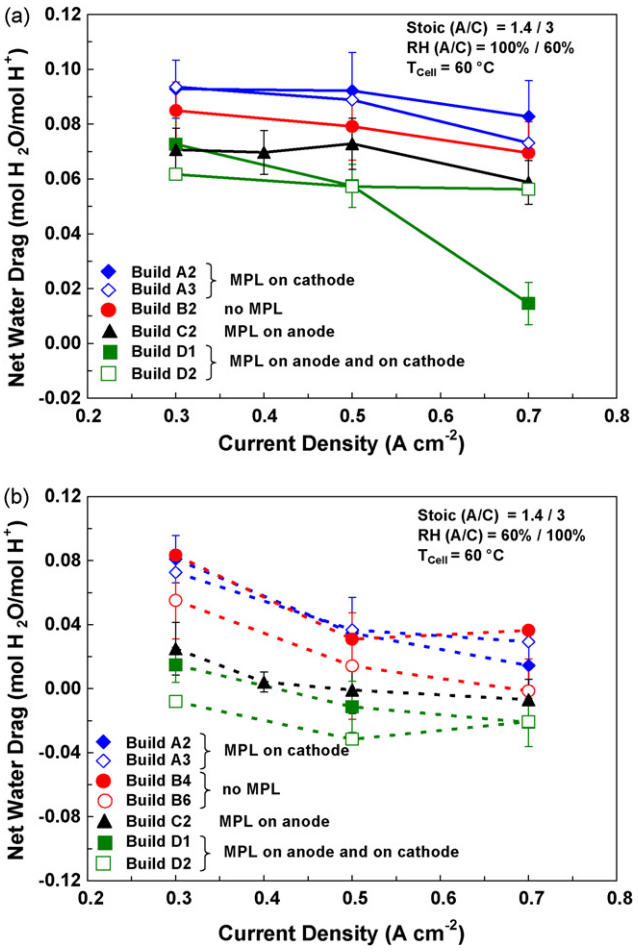

Fig. 6. Net water drag coefficients for builds with various combinations of porous transport layers at stoichiometric ratio of H_2/air of 1.4/3 for (a) anode/cathode relative humidity of 100/60% and (b) anode/cathode relative humidity of 60/100%. Error bars for builds A2, B2, B6, C2 and D1 are only shown for ease of comparison.

tested. However, more fluctuations in cell voltage, as indicated by the error bars, were noticed for the cell builds B2 and B6 (without a MPL) in Fig. 4 and when the fuel cell was operated at a stoichiometric ratio of H_2/air of 1.4/2 (Fig. 5). The error bars that are not visible in the figures are smaller than the symbols indicating small uncertainty in the results. Both standard polarization curves (Fig. 3) and cell performance curves at the water transport conditions (Fig. 4) clearly indicate that cells with a MPL displayed a better overall performance and durability and less variability than those without a MPL.

4.3. Effect of the MPL on net water drag

Fig. 6 presents the net drag coefficient of water from the anode to the cathode, α (mol H_2O (mol H^+)$^{-1}$), for all cases considered at a stoichiometric ratio of H_2/air of 1.4/3. The data is grouped according to inlet humidification conditions: A/C RH = 100/60% (Fig. 6a) and A/C RH = 60/100% (Fig. 6b). The scales on the two sub-figures are different. Only error bars that show typical experimental uncertainty from representative builds A2, B2, B6, C2 and D1 are included in the figure for ease of comparison.

The net drag coefficient was determined from water balance measurements at an average fuel cell operation of 23 h at each current density tested. The overall water balance consistently closed to within 5%. The absolute average relative error in water balance for all runs was 1.5%. The net drag coefficient was between 0.01 and 0.11 mol H_2O (mol H^+)$^{-1}$ for cell builds at A/C RH of 100/60% (Fig. 6a). However, it was lower when the cathode was at a higher humidification level than the anode (A/C RH of 60/100%) in Fig. 6b. This corresponding change in the drag coefficient as a result of change in the RH difference between the anode and the cathode provided confidence in the reliability of the measurements. This is consistent with results presented by other researchers [27–31] who reported a lower net drag coefficient when the cathode was at a higher humidification level than the anode. In the present study, as water is removed from the anode PTL into the unsaturated (60% RH) anode feed, it would be expected that there would be an increase in the back-diffusion of water from the cathode to the anode near the inlet of the flow filed. The difference in the net drag coefficient for the two combinations of RH is larger at higher current densities (Fig. 6a and b). This could be because the nitrogen in the 60% RH air feed at 0.7 A cm^{-2} would have 2.33 times the capacity to remove water and increase the net water transport from anode to cathode compared to the flow of nitrogen in the feed at 0.3 A cm^{-2}. On the other hand, the nitrogen in the 100% RH air feed would not pick up additional water compared to the 60% RH hydrogen stream, which tend to decrease the net water transport from anode to cathode.

The results of Fig. 6 also demonstrates that there is inherent variability in the performance of seemingly similar fuel cells, and accounting for measurement errors and the inherent performance variability, the difference in net drag is statistically insignificant. It is also important to note the comparable performance between similar cell builds (A2, A3), (B4, B6) and (D1, D2) and between the different builds with and without a MPL.

For the inlet A/C RH of 100/60%, builds A2 and A3 (MPL on cathode) show reproducible performance at 0.3 and 0.5 A cm^{-2} although small, significant variability can be observed at higher current density of 0.7 A cm^{-2} (Fig. 6a). Builds D1 and D2 (MPL on both electrodes) show reproducible performance at 0.5 A cm^{-2} and less variability at 0.3 than at 0.7 A cm^{-2}. The results of the net drag coefficient of one fuel cell build fall within the experimental uncertainty of the other as seen by the overlapping error bars.

For the case of inlet RH for A/C of 60/100% (Fig. 6b), builds A2 and A3 (MPL on cathode) show reproducible performance at 0.3 A cm^{-2} and a small variability at 0.5 and 0.7 A cm^{-2}. Builds D1 and D2 (MPL on both electrodes) show reproducible performance only at 0.7 A cm^{-2}. However, build D2 exhibits significantly lower net water drag than build D1 at 0.7 A cm^{-2} which we cannot explain at this time. Builds B4 and B6 (without a MPL) show a significant variability from each other although the drag coefficient from both cells falls within the experimental uncertainty of the results. The water drag for build B4 (without a MPL) at each current density lines up closely with data for at

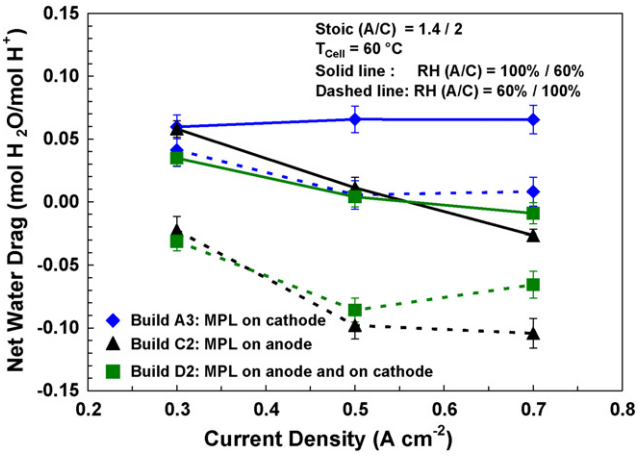

Fig. 7. Net water drag coefficients for builds with various combinations of porous transport layers at stoichiometric ratio of H_2/air of 1.4/2.

least one of the two builds A2 or A3 (MPL on cathode). The water drag for build C2 (MPL on anode) lines up closely with data from build D1 (MPL on both electrodes) at 0.3 and 0.5 A cm^{-2} and with data from build B6 (without a MPL) at 0.7 A cm^{-2}. This clearly showed that there is some variability in the fuel cell performance from one build to another. It also indicated that the addition of a MPL to the carbon fibre paper PTL at the cathode, however, did not cause a statistically significant change to the overall drag coefficient although there was a significant improvement to the fuel cell performance and durability when a MPL was used.

The net drag coefficients from water balance experiments carried at a H_2/air stoichiometric ratio of 1.4/2 and two combinations of A/C RH (100/60% and 60/100%) are shown in Fig. 7. Fuel cell builds without a MPL were unstable at this stoichiometric ratio and measurements were not obtained. The change in the RH difference between the anode and the cathode resulted in the corresponding change in the drag coefficient as is seen at a H_2/air stoichiometric ratio of 1.4/3 (Fig. 6). The presence of a MPL at the anode by itself or in combination with a MPL on the cathode appeared to cause a decrease in the net drag coefficient compared to when the MPL was only at the cathode. This is clearer at current densities above 0.5 A cm^{-2}. For the case of inlet RH for A/C of 60/100% and at a H_2/air stoichiometric ratio of 1.4/2 (Fig. 7), the net drag coefficient for build A3 (MPL on cathode) was significantly higher than for both builds C2 (MPL on anode) and D2 (MPL on both electrodes). For the inlet A/C RH of 100/60%, the net drag coefficient was higher for build A3 compared to builds C2 and D2 when the current density was above 0.5 A cm^{-2}. In general, the net drag coefficients at a H_2/air stoichiometric ratio of 1.4/2 were lower than at a ratio of 1.4/3. This is attributed to the fact that less air is fed to the fuel cell at lower stoichiometric ratio and the capacity of air to remove water is reduced.

The experimental results from previous studies on water transport in PEMFCs showed some common trends in the effect of operating conditions on net water drag [27–31]. However, the wide range of operating conditions and/or the different fuel cell components used make the comparison between these studies difficult. The main points from each of the previous experimental studies are discussed below.

Janssen and Overvelde [28] studied water transport in PEMFC and measured water drag for cells with different types of MEAs, though none using CCMs. The MEAs (50 cm^2) were made from Nafion 112 and Nafion 105. The fuel cell was operated in a counter flow configuration between 60 and 80 °C with gases pressure of 150 and 300 kPa. The net drag coefficient was calculated from water collected at the anode with fuel cell operated for more than 6 h at each of the only two current densities tested (0.4 and 0.6 A cm^{-2}). The gases used were either dry or fully saturated. Janssen and Overvelde [28] showed that the drag coefficient with the thinner membrane (Nafion 112) was lower than with Nafion 105 at the same operating conditions. The only results for Nafion 112 membrane were presented at a current density of 0.4 A cm^{-2} with similar E-Tek electrodes and MPLs on the electrode side and channels side. The net drag coefficients dropped from 0.07 to −0.20 mol H_2O (mol H^+)$^{-1}$ when the A/C RH was changed from 100/0% to 0/100% at a H_2/air stoichiometric ratio of 1.5/2. These values of drag coefficients cannot be compared with our results due to differences in the components used in the fuel cell as well as the operating conditions.

At 60 °C, the fuel cell with a MPL on both electrodes was unstable at current densities of 0.4 and 0.6 A cm^{-2} when both inlet gases were dry [28]. However for the same range of current density, the cell was able to operate with the double-sided MPL on both electrodes. Janssen and Overvelde [28] speculated that at these dry gases conditions, the presence of a MPL at the electrode and channel sides presents a buffer between the dry gas channel and the wet membrane. They also noticed a minor effect on the water transport with the different types of electrodes used at a H_2/air stoichiometric ratio of 1.5/2. However, at a H_2/air stoichiometric ratio of 4/2, a larger difference in the net drag was shown with the different electrodes. Their data could not allow a direct investigation of the effect of the MPL on the water drag coefficient because the PTL type and/or the catalyst loading for any two sets of their experiments were different.

Yan et al. [29] studied water transport in a PEMFC using a 25 cm^2 MEA from E-Tek with Nafion 117 and 1 mg cm^{-2} platinum catalyst loading at 80 °C and 101.3 kPa. The H_2/air stoichiometric ratio was 2/2. The PTL used was not mentioned in their study. They found that the net water drag coefficient decreased from 0.37 to 0.30 mol H_2O (mol H^+)$^{-1}$ with an increase in the current density from 0.3 to 0.7 A cm^{-2} at A/C RH of 100/60%. For the A/C RH 60/100% case, the net water drag coefficient decreased from 0.42 to 0.34 mol H_2O (mol H^+)$^{-1}$ with an increase in the current density from 0.3 to 0.5 A cm^{-2}.

Cai et al. [30] presented results on net water drag at two different combination of A/C RH (0/56% and 75/56%) and H_2/air stoichiometric ratio of 1.1/2.5. The fuel cell was operated at 60 °C and 202.6 kPa. The MEA used has an active area of 128 cm^2 and was made of Nafion 112 and homemade electrodes made of a backing layer, a MPL and a catalyst layer. Similar electrodes were used at the anode and cathode. The net drag coefficient was calculated from water collected during 2 h of operation. Cai et al. [30] reported net drag coefficients drop from

−0.03 to −0.06 mol H_2O (mol H^+)$^{-1}$ when the current density increased from 0.3 to 0.6 A cm^{-2} for A/C RH of 75/56% and from −0.06 to −0.09 mol H_2O (mol H^+)$^{-1}$ for the A/C RH of 0/56%. They concluded that the net amount of water transport across the membrane was from cathode to anode whether anode was humidified or not. Although the conclusion is correct at the conditions studied, it could be misleading because the effect of various RH on the cathode side was not considered. In our study, when the current density was between 0.3 and 0.5 A cm^{-2}, positive net drag coefficients were obtained for the builds with a MPL on both electrodes (D1 and D2) for A/C RH of 100/60% at both stoichiometric ratios of H_2/air (Figs. 6a and 7). However, negative drag coefficients were obtained for A/C RH of 60/100% at current densities above 0.5 A cm^{-2} (Fig. 6b). This shows that the net water transport across the membrane was from cathode to anode when the cathode was fully humidified. This clearly shows that the difference in operating conditions and fuel cell components will result in a different water drag coefficients.

Murahashi et al. [31] studied water transport in PEMFC and compared model predictions to the experimental water drag results of a 25 cm^2 active area MEA made from Nafion 112 with platinum loading of 0.5 mg cm^{-2}. A MPL was used on both electrodes. The FFP used was made of one serpentine channel. The cell was operated in a counter flow configuration at 80 °C and a H_2/air stoichiometric ratio of 1.4/2. The net drag coefficients at 0.3 mA cm^{-2} and anode RH of 42% decreased from 0.08 to −0.10 mol H_2O (mol H^+)$^{-1}$ when the cathode RH was increased from 42% to 80%. These were the only experimental data reported in their study. In addition, Murahashi et al. [31] used a 2D cell model that accounted for the change in the gas content related to the flow configuration, the humidity of the supply gas, reaction rates, the mass balance of each gas species along the flow channels and the capillary effect due to the presence of the MPL. Their model over predicted the net drag coefficients and revealed that the drag coefficient varies along the channel. This indicates that local conditions within a fuel cell may be such that water may indeed be dragged in opposite direction at two different locations as has also been recently reported [34,35]. Murahashi et al. [31] suggested that the hydrophobic MPLs small micro pores hold and keep liquid water, which humidifies the membrane and catalyst layer and allows stable fuel cell operation even under dry air conditions.

4.4. Effect of the MPL on cell resistance

Figs. 8 and 9 show the internal cell resistance of cell builds with and without a MPL at various current densities. The internal cell resistance was measured at the water balance experimental conditions (Section 2.4) to check if there is a correlation between the net water drag and the measured internal cell resistance. It can be seen from both figures that there is variability between similar fuel cell builds and between the various builds. The internal cell resistance tends to increase with increasing current densities for both inlet humidification conditions and at both H_2/air stoichiometric ratios (Figs. 8 and 9). However, the internal cell resistance for only one build with a MPL on the cathode (A3) slightly decreased with increasing the current density for the

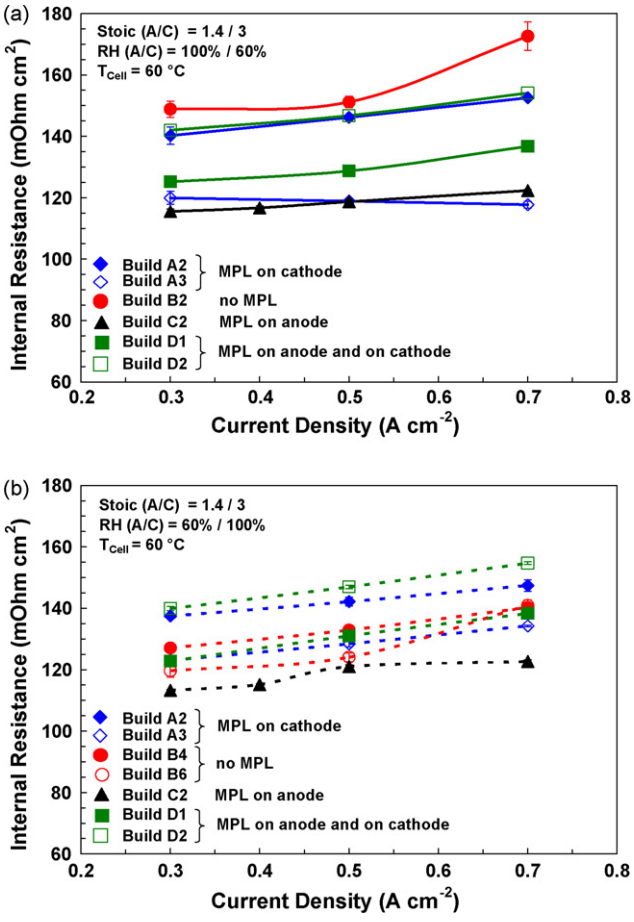

Fig. 8. Cell internal resistance for builds with various combinations of porous transport layers at stoichiometric ratio of H_2/air of 1.4/3 for (a) anode/cathode relative humidity of 100/60% and (b) anode/cathode relative humidity of 60/100%. Error bars not visible are smaller than the symbols.

case with an A/C RH of 100/60% and a H_2/air stoichiometric ratio of 1.4/3 (Fig. 8a), and for both humidification conditions at a H_2/air stoichiometric ratio of 1.4/2 (Fig. 9).

The internal cell resistance for builds A3, C2 and D2 were slightly lower at H_2/air stoichiometric ratio of 1.4/2 (Fig. 9)

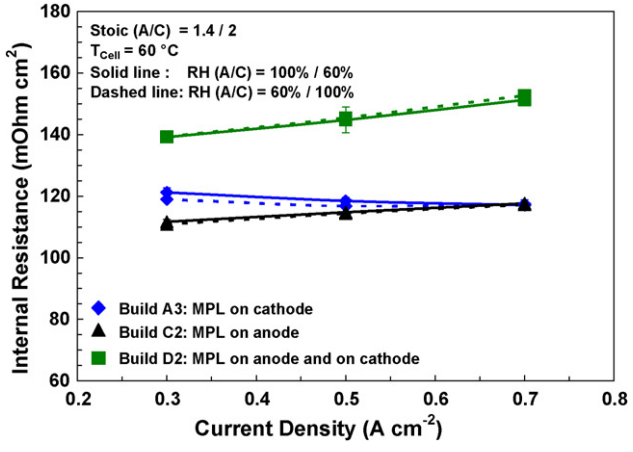

Fig. 9. Cell internal resistance for builds with various combinations of porous transport layers at stoichiometric ratio of H_2/air of 1.4/2. Error bars not visible are smaller than the symbols.

compared to a ratio of 1.4/3 (Fig. 8). This might indicate that the membrane is better humidified at the H_2/air stoichiometric ratio of 1.4/2. In addition, the internal cell resistance values for builds A3 and C2 were lower than those for build D2 at both H_2/air stoichiometric ratios tested (Figs. 8 and 9). The tested RH difference between the anode and the cathode suggests an insignificant effect of RH on the internal resistance which is clearly shown in Fig. 9. However, the difference in the A/C RH was shown to have a significant effect on the net drag coefficient (Figs. 6 and 7). There is no clear correlation between the net water drag and the measured internal resistance that can be seen from our results at the conditions studied.

Yan et al. [29] noticed with the Nafion 117 membrane that the membrane resistance was a strong function of the feed gas RH. Cai et al. [30] showed that when Nafion 112 was used in the cell, the membrane resistance and fuel cell performance were not sensitive to anode humidity at cathode RH of 56%. They also reported a slight variation in the internal cell resistance (from 221 to 216 $m\Omega\,cm^2$) at 0.5 $A\,cm^{-2}$ when the anode RH was increased from 0 to 100%, while the cathode RH remained at 56%. In our study, the internal cell resistance for builds with a MPL did not vary significantly with either combination of A/C RH.

In summary, we directly measured the influence of MPL on water drag coefficient via sets of experiments differing only in the presence of MPL or not. Our results show that at the operating conditions studied, the overall net water drag coefficient is not affected by whether a MPL is used or not in the fuel cell, although the presence of a MPL significantly improves the fuel cell performance and durability. In addition, the overall net water drag coefficient is strongly affected by the operating conditions. Our experimental results do not support the frequently asserted hypothesis [17,19] that the MPL enhances back diffusion of water from the cathode to the anode. This suggests that the mechanism by which the MPL improves the overall cell performance is more complex than has been previously proposed. Further research is ongoing to reveal the mechanism by which the MPL influence the overall cell performance.

5. Conclusions

The effect of a microporous layer on the overall net water transport in a standard 100 cm^2 active area PEM fuel cell was experimentally investigated. Cells with a MPL on either electrode or on both electrodes exhibited better overall performance and durability compared to cells without a MPL. Water balance measurements that were consistently accurate to within 5% were employed to determine the net drag coefficient. As would be expected, the net drag coefficient was lower when the inlet anode/cathode RH was 60/100%, compared to 100/60% for the three current densities (0.3, 0.5 and 0.7 $A\,cm^{-2}$) and two stoichiometric ratios of H_2/air (1.4/3 and 1.4/2) studied. However, there was no statistically significant difference in the net drag coefficient for cells with a MPL at the cathode and no MPL on the anode compared to cells without a MPL at the conditions studied. The presence of a MPL at either the anode by itself or in combination with a MPL on the cathode appeared to cause a decrease in the net water drag compared with cells with a MPL only at the cathode when the H_2/air stoichiometric ratio was 1.4/2.

The results indicate that the function of the MPL in improving fuel cell performance is not associated with overall water drag as has been proposed by some researchers. Further work is required to reveal the mechanism by which the presence of the MPL affects PEM fuel cell performance.

Acknowledgement

This work was partially funded through a Natural Science and Engineering Council of Canada (NSERC) Collaborative Research Grant in partnership with E.I. Du Pont of Canada Research and Development.

References

[1] T.A. Zawodzinski, C. Derouin, S. Radzinski, R.J. Sherman, T. van Smith, T.E. Springer, S. Gottesfeld, J. Electrochem. Soc. 140 (1993) 1041–1047.
[2] D.P. Wilkinson, H.H. Voss, K. Prater, J. Power Sources 49 (1994) 117–127.
[3] P. Berg, K. Promislow, J.St. Pierre, J. Stumper, B. Wetton, J. Electrochem. Soc. 151 (2004) A341–A353.
[4] J.G. Pharoah, K. Karan, W. Sun, J. Power Sources 161 (2006) 214–224.
[5] P. Staiti, Z. Poltarzewski, V. Alderucci, G. Maggio, N. Giordano, A. Fasulo, J. Appl. Electrochem. 22 (1992) 663–667.
[6] M. Mathias, J. Roth, J. Fleming, W. Lehnert, in: W. Vielstich, A. Lamm, H. Gasteiger (Eds.), Handbook of Fuel Cells—Fundamentals, Technology and Applications, vol. 3, John Wiley & Sons, New York, 2003, pp. 1–21.
[7] J.T. Gostick, M.W. Fowler, M.A. Ioannidis, M.D. Pritzker, Y.M. Volfkovich, A. Sakars, J. Power Sources 156 (2006) 375–387.
[8] D.M. Bernardi, M.W. Verbrugge, J. Electrochem. Soc. 137 (1990) 3344–3350.
[9] D.M. Bernardi, M.W. Verbrugge, J. Electrochem. Soc. 139 (1992) 2477–2491.
[10] T.V. Nguyen, R.E. White, J. Electrochem. Soc. 140 (1993) 2178–2186.
[11] T.F. Fuller, J. Newman, J. Electrochem. Soc. 140 (1993) 1218–1225.
[12] Z.H. Wang, C.Y. Wang, K.S. Chen, J. Power Sources 94 (2001) 40–50.
[13] L. You, H.T. Liu, Int. J. Heat Mass Transfer 45 (2002) 2277–2287.
[14] G.J.M. Janssen, J. Electrochem. Soc. 148 (2001) A1313–A1323.
[15] J.H. Nam, M. Kaviany, Int. J. Heat Mass Transfer 46 (2003) 4595–4611.
[16] U. Pasaogullari, C.-Y. Wang, Electrochim. Acta 49 (2004) 4359–4369.
[17] A.Z. Weber, J. Newman, J. Electrochem. Soc. 152 (2005) A677–A688.
[18] Z. Qi, A. Kaufman, J. Power Sources 109 (2002) 38–46.
[19] G. Lin, T.V. Nguyen, J. Electrochem. Soc. 153 (2006) A372–A382.
[20] U. Pasaogullari, C.-Y. Wang, K.S. Chen, J. Electrochem. Soc. 152 (2005) A1574–A1582.
[21] V.A. Paganin, E.A. Ticianelli, E.R. Gonzalez, J. Appl. Electrochem. 26 (1996) 297–304.
[22] L.R. Jordan, A.K. Shukla, T. Behrsing, N.R. Avery, B.C. Muddle, M. Forsyth, J. Power Sources 86 (2000) 250–254.
[23] J.M. Song, S.Y. Cha, W.M. Lee, J. Power Sources 94 (2001) 78–84.
[24] E. Antolini, R.R. Passos, E.A. Ticianelli, J. Appl. Electrochem. 32 (2002) 383–388.
[25] J. Chen, T. Matsuura, M. Hori, J. Power Sources 131 (2004) 155–161.
[26] X.L. Wang, H.M. Zhang, J.L. Zhang, H.F. Xu, Z.Q. Tian, J. Chen, H.X. Zhonga, Y.M. Liang, B.L. Yi, Electrochim. Acta 51 (2006) 4909–4915.
[27] K.-H. Choi, D.-H. Peck, C.S. Kim, D.-R. Shin, T.-H. Lee, J. Power Sources 86 (2000) 197–201.
[28] G.J.M. Janssen, M.L.J. Overvelde, J. Power Sources 101 (2001) 117–125.
[29] Q. Yan, H. Toghiani, J. Wu, J. Power Sources 158 (2006) 316–325.

[30] Y. Cai, J. Hu, H. Ma, B. Yi, H. Zhang, Electrochim. Acta 51 (2006) 6361–6366.
[31] T. Murahashi, M. Naiki, E. Nishiyama, J. Power Sources 162 (2006) 1130–1136.
[32] K. Karan, H. Atiyeh, A. Phoenix, E. Halliop, J. Pharoah, B. Peppley, Electrochem. Solid-State Lett. 10 (2007) B34–B38.
[33] SGL Carbon Group, Fuel Cell Components: SIGRACET. Website: (http://www.sglcarbon.com/sgl_t/fuelcell/pdf/SIGRACET_GDL_10.pdf) site visited March 7, 2007.
[34] Q. Dong, M.M. Mench, S. Cleghorn, U. Beuscher, J. Electrochem. Soc. 152 (2005) A2114–A2122.
[35] G.Q. Lu, F.Q. Liu, C.Y. Wang, J. Power Sources 164 (2007) 134–140.